Preprints of the 21st IFAC World Congress (Virtual)
Berlin, Germany, July 12-17, 2020

Time-Energy Efficient Finite Time Attitude Tracking Control of Spacecraft Using Disturbance Observer

Syed Muhammad Amrr * **Arunava Banerjee** * **M. Nabi** *

* *Department of Electrical Engineering, Indian Institute of Technology Delhi, New Delhi 110016, India. (e-mail: syedamrr@gmail.com, arunavabanerjee27@gmail.com, mnabi@ee.iitd.ac.in).*

Abstract: In this paper, the attitude controller of spacecraft tracks the time-energy near-optimal angular velocity generated by the Legendre Pseudospectral method (LPSM). The near-optimal reference trajectory is obtained offline by applying the LPSM on the nominal spacecraft dynamics, which is without noises and disturbances. The proposed tracking control scheme works online, and along with the tracking of the near-optimal path, it also rejects the external disturbances and noises. The composite control law is developed by combining the sliding mode control (SMC) and the output of a finite-time disturbance observer. The SMC ensures the finite tie results whereas the disturbance observer helps in avoiding the chattering in control. The stability analysis of relative dynamics under the proposed scheme guarantees the convergence of sliding surface and relative states in finite-time. The simulation analysis further illustrates the effective performance of the proposed strategy.

Keywords: Pseudospectral method, finite time theory, disturbance observer, sliding mode control, rigid spacecraft

1. INTRODUCTION

In the past few decades, various control techniques have been applied to the challenging spacecraft problems owing to its complex and nonlinear dynamics (Krstic and Tsiotras, 1999; Luo et al., 2005a; Sahoo et al., 2016; Amrr et al., 2019; Amrr and Nabi, 2019). Moreover, the spacecraft missions require features like higher accuracy, faster convergence, better steady-state precision, and fuel efficiency, etc., which makes the controller design more challenging. Disturbance rejection property in the attitude control design is also an essential aspect of the space mission. Different robust control techniques have also been used to attenuate the disturbances in the spacecraft like sliding mode control (SMC) schemes (Tiwari et al., 2018; Ma, 2013), adaptive control (Sahoo et al., 2016; Zhu et al., 2011), disturbance observer-based control (Yan and Wu, 2017), and references therein. These schemes have not explored the optimal aspect of the control system.

The optimal control strategies have been proposed for the spacecraft system in (Luo et al., 2005b; Feng et al., 2016; Taheri and Junkins, 2018). However, the formulation of optimal control design in these approaches are complex and need comprehensive mathematical analysis. A relatively new optimal control method called Legendre Pseudospectral method (LPSM) has been applied to solve a wide range of nonlinear real-time problems, including the problem related to the spacecraft missions (Zhou et al., 2012; Ge et al., 2017; Banerjee et al., 2019a,b, 2020). This method converts the original continuous-time optimal control problem into its equivalent nonlinear programming problem, which then becomes much more easier to tackle. The ease of implementation and a relatively faster convergence rate makes it the method of choice for a wide range of problems (Garg et al., 2010; Banerjee et al., 2020). In Banerjee et al. (2019a), the LPSM has been applied to the rigid spacecraft to obtain the time-energy optimal state response, and this same strategy has been used in this work to generate time-energy near-optimal reference trajectories. This reference trajectory generation is produced offline.

The proposed algorithm incorporates both robust and optimal strategies to achieve better disturbance rejection and optimal convergence of the closed loop system. Therefore, a robust control law is proposed, whose objective is to track that reference trajectories while rejecting the noises and disturbances it encounters on its path. The proposed tracking control law is designed by combining the robust nonlinear disturbance observer (RNDO) with a non-singular terminal SMC (NSTSMC) scheme (Eshghi and Varatharajoo, 2018; Qiao et al., 2020). The output of RNDO estimates the actual disturbance, then supplies it to the controller for compensating the disturbance in the spacecraft dynamics. Most of the disturbance gets attenuated by the output of the RNDO. Thus, the RNDO also helps in reducing the use of high gain switching control in the SMC design, which in turn alleviates the chattering problem.

The key contributions of this work are outlined as

- The attitude tracking of time-energy near-optimal trajectory obtained from LPSM as a reference trajectory for the attitude regulation of spacecraft subjected to the disturbances and noises.

- The RNDO, used as a disturbance rejection, estimates the disturbance in finite-time and also helps in alleviating the chattering phenomenon.
- The proposed composite control, which consists of RNDO and NSTSMC, guarantees the finite-time convergence of sliding surface as well as the closed-loop system states.
- The numerical simulation analysis validates the efficacy of the designed scheme.

2. PROBLEM FORMULATION

The kinematic and dynamic equations of the spacecraft is modelled as (Wu and Cao, 2017)

$$\dot{q}_0 = -0.5\boldsymbol{q}_v^T\boldsymbol{w}, \quad \dot{\boldsymbol{q}}_v = 0.5(q_0\boldsymbol{I} + \boldsymbol{q}_v^\times)\boldsymbol{w}, \tag{1a}$$

$$\boldsymbol{J}\dot{\boldsymbol{w}} = -\boldsymbol{w}^\times\boldsymbol{J}\boldsymbol{w} + \boldsymbol{u} + \boldsymbol{d}. \tag{1b}$$

where $q_0 \in \mathbb{R}$, $\boldsymbol{q}_v = [q_1\ q_2\ q_3]^T \in \mathbb{R}^3$ are the scalar and vector quaternion, respectively and $\boldsymbol{q} \in \mathbb{R}\times\mathbb{R}^3 = (q_0, \boldsymbol{q}_v^T)^T$ is the unit quaternions representation, which satisfies the unity constraint $q_0^2 + \boldsymbol{q}_v^T\boldsymbol{q}_v = 1$. The variable $\boldsymbol{w} \in \mathbb{R}^3$ denotes the angular velocity, $\boldsymbol{I} \in \mathbb{R}^{3\times3}$ describes the identity matrix, $\boldsymbol{J} \in \mathbb{R}^{3\times3}$ is the inertia matrix, $\boldsymbol{d} \in \mathbb{R}^3$ represents the external disturbance, and $\boldsymbol{u} \in \mathbb{R}^3$ is the control input. The notation $(\cdot)^\times \in \mathbb{R}^{3\times3}$ represents the skew symmetric matrix acting on a vector.

Similar to (1a), the motion of near-optimal reference attitude is governed by $\dot{q}_{r0} = -0.5\boldsymbol{q}_{rv}^T\boldsymbol{w}_r$ and $\dot{\boldsymbol{q}}_{rv} = 0.5(q_{r0}\boldsymbol{I} + \boldsymbol{q}_{rv}^\times)\boldsymbol{w}_r$, where q_{r0} and $\boldsymbol{q}_{rv}$ are the scalar and vector near-optimal reference quaternions, respectively and $\boldsymbol{q}_r = (q_{r0}, \boldsymbol{q}_{rv}^T)^T \in \mathbb{R}\times\mathbb{R}^3$. The near-optimal reference angular velocity is denoted by $\boldsymbol{w}_r$, which is obtained offline from the LPSM (Banerjee et al., 2019a).

The relative attitude quaternion between the body frame and the near-optimal reference frame is expressed as $\boldsymbol{q}_e = (q_{e0}, \boldsymbol{q}_{ev}^T)^T \in \mathbb{R}\times\mathbb{R}^3$. The relative quaternion are determined as (Tiwari et al., 2018)

$$q_{e0} = \boldsymbol{q}_{rv}^T\boldsymbol{q}_v + q_0q_{r0}; \quad \boldsymbol{q}_{ev} = q_{r0}\boldsymbol{q}_v - \boldsymbol{q}_{rv}^\times\boldsymbol{q}_v - q_0\boldsymbol{q}_{rv}. \tag{2}$$

The relative quaternion also satisfies the unity constraint (Tiwari et al., 2018). The relative angular velocity is defined as

$$\boldsymbol{w}_e = \boldsymbol{w} - \boldsymbol{w}_r. \tag{3}$$

In view of (1), (2), and (3), the relative error dynamics can be written as

$$\dot{q}_{e0} = -0.5\boldsymbol{q}_{ev}^T\boldsymbol{w}_e, \tag{4a}$$

$$\dot{\boldsymbol{q}}_{ev} = +0.5(q_{e0}\boldsymbol{I} + \boldsymbol{q}_{ev}^\times)\boldsymbol{w}_e, \tag{4b}$$

$$\boldsymbol{J}\dot{\boldsymbol{w}}_e = -\boldsymbol{w}^\times\boldsymbol{J}\boldsymbol{w} - \boldsymbol{J}\dot{\boldsymbol{w}}_r + \boldsymbol{u} + \boldsymbol{d}. \tag{4c}$$

2.1 Problem Statement

The objective of this work is to propose a robust attitude controller scheme for the tracking of reference trajectory generated by the LPSM (Banerjee et al., 2019a). The performance index minimized after application of LPSM is given as:

$$\mathcal{J} = t_f + \int_0^{t_f} \boldsymbol{u}^T\mathcal{R}\boldsymbol{u}d\tau, \tag{5}$$

where $\mathcal{R} \in \mathbb{R}^{3\times3}$ denotes a weight matrix, which is positive definite, and t_f represents the final time. The cost function (5) minimizes the combination of time and energy consumption by the spacecraft.

While tracking this time-energy near-optimal reference trajectory, the proposed control law must also provide the robustness against disturbances and converge the relative system states to the origin in finite-time. Mathematically, it can be expressed as:

$$\lim_{t\to t_f} q_{e0} = 1; \ \lim_{t\to t_f} \boldsymbol{q}_{ev} = [0\ 0\ 0]^T; \ \lim_{t\to t_f} \boldsymbol{w}_e = [0\ 0\ 0]^T.$$

The following assumption has been considered for the problem.

Assumption 1. The disturbance in the dynamics is considered to be bounded, but with unknown bound. Further, the $\dot{\boldsymbol{d}}$ is also considered to be bounded, i.e., $\|\dot{\boldsymbol{d}}\| \le \varpi$, where $\varpi > 0$ is a constant.

3. PROPOSED ATTITUDE CONTROL STRATEGY

The overall control scheme for the attitude tracking of near-optimal reference trajectory from the LPSM is shown in Fig. 1. The attitude control is designed by combining the output of the RNDO and the SMC. The RNDO scheme estimates the disturbance in the system and feed forward it to the composite controller for disturbance compensation. Therefore, not using the high gain switching control for disturbance rejection helps in avoiding the chattering problem. Moreover, the SMC approach is adopted to establish the finite-time results of system states. The proposed RNDO and SMC approaches are given in the subsequent section.

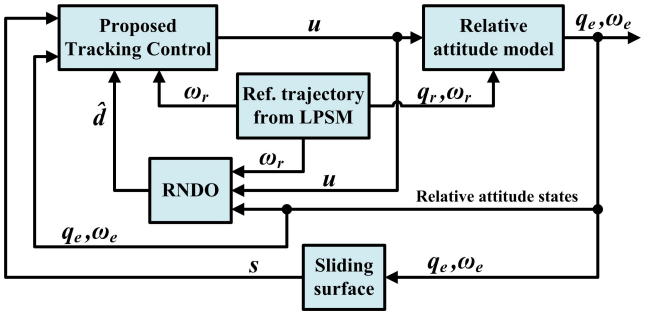

Fig. 1. Schematic diagram of the developed scheme.

3.1 Disturbance observer design

The proposed RNDO (6) produces the estimate of $\boldsymbol{d}$ in terms of $\hat{\boldsymbol{d}} \in \mathbb{R}^3$ using an auxiliary dynamics of variable $\boldsymbol{z} \in \mathbb{R}^3$ (6b). The RNDO model is expressed as

$$\hat{\boldsymbol{d}} = \boldsymbol{z} + \mu_1\boldsymbol{J}\boldsymbol{w}_e - \mu_2\int_0^t \mathbf{sgn}^\rho(\boldsymbol{\Omega})\ d\tau, \tag{6a}$$

$$\dot{\boldsymbol{z}} = -\mu_1\{-\boldsymbol{w}^\times\boldsymbol{J}\boldsymbol{w} - \boldsymbol{J}\dot{\boldsymbol{w}}_r + \boldsymbol{u} + \hat{\boldsymbol{d}}\}, \tag{6b}$$

where $\rho \in (0,1)$, $\mu_1 > 0$ and $\mu_2 \ge \varpi$ are the RNDO gains. Moreover, variable $\boldsymbol{\Omega} \in \mathbb{R}^3$ is given as:

$$\boldsymbol{\Omega} = \hat{\boldsymbol{d}} - \boldsymbol{J}\dot{\boldsymbol{w}}_e - \boldsymbol{w}^\times\boldsymbol{J}\boldsymbol{w} - \boldsymbol{J}\dot{\boldsymbol{w}}_r + \boldsymbol{u}, \tag{7}$$

and function $\mathbf{sgn}^\rho(\boldsymbol{\Omega}) \in \mathbb{R}^3$ is expressed as:

$$\mathbf{sgn}^\rho(\boldsymbol{\Omega}) = \left[|\Omega_1|^\rho \operatorname{sign}(\Omega_1), |\Omega_2|^\rho \operatorname{sign}(\Omega_2), |\Omega_3|^\rho \operatorname{sign}(\Omega_3)\right]^T$$

The finite-time convergence of the proposed RNDO is proved using the following Lemma.

Lemma 1. (Yu et al., 2005) Consider a continuous function $\dot{\vartheta} = g(\vartheta)$, $\vartheta \in \mathbb{R}^n$ with 0 as equilibrium point, and a Lyapunov function $V(\vartheta) : \mathbb{R}^n \to \mathbb{R}$ defined in an open neighbourhood $U_0 \subseteq \mathbb{R}^n$ of the origin. For $\gamma_1 > 0$, $\gamma_2 > 0$, and $\rho \in (0, 1)$, if the following inequality holds

$$\dot{V}(\vartheta) \leq -\gamma_2 V(\vartheta) - \gamma_1 V^{\rho}(\vartheta), \quad \vartheta \in U_0, \tag{8}$$

then variable ϑ will be forced to 0 in finite-time with $t_{settling} \leq \frac{1}{\gamma_2(1-\rho)} \ln\left\{\frac{\gamma_2 V^{1-\rho}(0)+\gamma_1}{\gamma_1}\right\}$.

Theorem 1. Considering the tracking dynamics (4) under the Assumption 1. The output of RNDO (6) will estimate $\boldsymbol{d}$ in finite-time. In other words, the disturbance estimation error ($\tilde{\boldsymbol{d}} = \hat{\boldsymbol{d}} - \boldsymbol{d}$) will be forced to zero in finite-time.

Proof. The value of $\boldsymbol{\Omega}$ can be equate to $\tilde{\boldsymbol{d}}$ by substituting $\boldsymbol{J}\dot{\boldsymbol{w}}_e$ from (4c) into (7). Moreover, the differentiation of $\tilde{\boldsymbol{d}}$ w.r.t. time can be obtained using (6a) as

$$\dot{\tilde{\boldsymbol{d}}} = \dot{\hat{\boldsymbol{d}}} - \dot{\boldsymbol{d}} = \{\dot{\boldsymbol{z}} + \mu_1 \boldsymbol{J}\dot{\boldsymbol{w}}_e - \mu_2 \mathbf{sgn}^{\rho}(\tilde{\boldsymbol{d}})\} - \dot{\boldsymbol{d}}. \tag{9}$$

The equation (9) can further be simplified by putting the expression of $\dot{\boldsymbol{z}}$ and $\boldsymbol{J}\dot{\boldsymbol{w}}_e$ in it to obtain

$$\dot{\tilde{\boldsymbol{d}}} = -\mu_1 \tilde{\boldsymbol{d}} - \mu_2 \mathbf{sgn}^{\rho}(\tilde{\boldsymbol{d}}) - \dot{\boldsymbol{d}}. \tag{10}$$

Now, select a Lyapunov candidate, which is a positive definite function of variable $\tilde{\boldsymbol{d}}$, as $V_0 = \frac{1}{2}\tilde{\boldsymbol{d}}^T\tilde{\boldsymbol{d}}$. The time derivative of V_0 using (10) yields

$$\begin{aligned}
\dot{V}_0 &= \tilde{\boldsymbol{d}}^T\dot{\tilde{\boldsymbol{d}}} = \tilde{\boldsymbol{d}}^T(-\mu_1\tilde{\boldsymbol{d}} - \mu_2\mathbf{sgn}^{\rho}(\tilde{\boldsymbol{d}}) - \dot{\boldsymbol{d}}),\\
&= -\mu_1\tilde{\boldsymbol{d}}^T\tilde{\boldsymbol{d}} - \mu_2\|\tilde{\boldsymbol{d}}\|\|\tilde{\boldsymbol{d}}\|^{\rho} - \tilde{\boldsymbol{d}}^T\dot{\boldsymbol{d}},\\
&\leq -\mu_1\|\tilde{\boldsymbol{d}}\|^2 - \mu_2\|\tilde{\boldsymbol{d}}\|^{1+\rho} + \|\tilde{\boldsymbol{d}}\|\|\dot{\boldsymbol{d}}\|.
\end{aligned} \tag{11}$$

Using $\|\dot{\boldsymbol{d}}\| \leq \varpi$ from Assumption 1 in (11) to obtain

$$\begin{aligned}
\dot{V}_0 &\leq -\mu_1\|\tilde{\boldsymbol{d}}\|^2 - \mu_2\|\tilde{\boldsymbol{d}}\|^{1+\rho} + \varpi\|\tilde{\boldsymbol{d}}\|,\\
&\leq -2\mu_1 V_0 - 2^{\frac{1+\rho}{2}}\mu_2 V_0^{\frac{1+\rho}{2}} + \sqrt{2}\,\varpi V_0^{\frac{1}{2}},\\
&= -\vartheta_1 V_0 - \vartheta_2 V_0^{\frac{1+\rho}{2}} + \vartheta_3 V_0^{\frac{1}{2}},\\
&= -\vartheta_1 V_0 - \left\{\vartheta_2 - \frac{\vartheta_3}{V_0^{\frac{\rho}{2}}}\right\} V_0^{\frac{1+\rho}{2}}.
\end{aligned} \tag{12}$$

where $\vartheta_1 = 2\mu_1 > 0$, $\vartheta_2 = 2^{\frac{1+\rho}{2}}\mu_2 > 0$, $\vartheta_3 = \sqrt{2}\,\varpi > 0$, and $\mu_2 > \varpi$. Correspondingly, in (12), $\left\{\vartheta_2 - \frac{\vartheta_3}{V_1^{\frac{\rho}{2}}}\right\} > 0$. Thus, equation (12) satisfies the inequality of *Lemma 1.* Therefore, variable $\tilde{\boldsymbol{d}}$ will converge to origin in finite-time and the residual bound of $\tilde{\boldsymbol{d}}$ is $\leq \frac{\sqrt{2}\vartheta_3^{1/\rho}}{\vartheta_2^{1/\rho}}$. Moreover, the selection of gain μ_2 such that $\vartheta_2 > \vartheta_3$ will ensure narrower residual set of $\tilde{\boldsymbol{d}}$.

3.2 Composite Control Design

The proposed controller is designed by employing $\hat{\boldsymbol{d}}$ from the previous subsection and a non-singular terminal sliding surface (NSTSS). The structure of NSTSS is proposed as:

$$\boldsymbol{s} = \boldsymbol{w}_e + a_1\mathbf{sgn}^{\varrho}(q_{e0}\boldsymbol{q}_{ev}) + a_2(q_{e0}\boldsymbol{q}_{ev}), \tag{13}$$

where $\boldsymbol{s} \in \mathbb{R}^3$ is a sliding manifold vector, a_1, a_2 are positive constants, and $\varrho \in (0, 1)$.

The time derivative of $\boldsymbol{J}\boldsymbol{s}$ yields

$$\begin{aligned}
\boldsymbol{J}\dot{\boldsymbol{s}} = &-\boldsymbol{w}^{\times}\boldsymbol{J}\boldsymbol{w} - \boldsymbol{J}\dot{\boldsymbol{w}}_r + \boldsymbol{u} + \boldsymbol{d} + \boldsymbol{J}\{a_1\varrho\,\mathrm{diag}(|q_{e0}\boldsymbol{q}_{ev}|^{\varrho-1})\\
&+ a_2\boldsymbol{I}\}\{-0.5\boldsymbol{q}_{ev}\boldsymbol{q}_{ev}^T + 0.5q_{e0}\left(q_{e0}\boldsymbol{I} + \boldsymbol{q}_{ev}^{\times}\right)\}\boldsymbol{w}_e.
\end{aligned} \tag{14}$$

The proposed composite attitude tracking control law is defined as:

$$\begin{aligned}
\boldsymbol{u} = &\boldsymbol{w}^{\times}\boldsymbol{J}\boldsymbol{w} + \boldsymbol{J}\dot{\boldsymbol{w}}_r - k\boldsymbol{s} - \boldsymbol{J}\{a_1\varrho\,\mathrm{diag}(|q_{e0}\boldsymbol{q}_{ev}|^{\varrho-1}) + a_2\boldsymbol{I}\}\\
&\times\{-0.5\boldsymbol{q}_{ev}\boldsymbol{q}_{ev}^T + 0.5q_{e0}\left(q_{e0}\boldsymbol{I} + \boldsymbol{q}_{ev}^{\times}\right)\}\boldsymbol{w}_e - \hat{\boldsymbol{d}}\\
&- \gamma\,\mathrm{sign}(\boldsymbol{s}).
\end{aligned} \tag{15}$$

where $k > 0$ is a gain constant and $\gamma > 0$ is a small switching gain constant. The switching gain is designed to restrict the random high-frequency noises of small magnitude for which the RNDO is not competent enough to estimate the high-frequency noises.

4. STABILITY ANALYSIS

In this section, the stability analysis is divided into two parts. In the first part, the finite-time convergence of sliding manifold is presented, and the second part guarantees the finite-time convergence of relative states. The given property is used in the stability proof.

Property 1. (Strang, 1993): For any vector $\boldsymbol{v} \in \mathbb{R}^3$ and symmetric matrix $\boldsymbol{J} \in \mathbb{R}^{3\times3}$, the following inequality always fulfilled: $\lambda_{\min}(\boldsymbol{J})\|\boldsymbol{v}\|^2 \leq \boldsymbol{v}^T\boldsymbol{J}\boldsymbol{v} \leq \lambda_{\max}(\boldsymbol{J})\|\boldsymbol{v}\|^2 \forall\ \boldsymbol{v}$, where $\lambda_{\max}(\boldsymbol{J})$ and $\lambda_{\min}(\boldsymbol{J})$ are the max. and min. positive eigenvalues of $\boldsymbol{J}$.

Theorem 2. Consider the relative dynamics of spacecraft (4), NSTSS (13), and the proposed composite control (15). The closed-loop system achieves

(i) the finite-time convergence of sliding manifold to zero,
(ii) as $\boldsymbol{s} \to 0$, the relative system states are also forced to their equilibrium point in finite-time.

Proof (i). Selecting a new Lyapunov candidate V_1 as

$$V_1 = \frac{1}{2}\boldsymbol{s}^T\boldsymbol{J}\boldsymbol{s}. \tag{16}$$

Substituting (14) in the time derivative of V_1 gives

$$\begin{aligned}
&\dot{V}_1 = \boldsymbol{s}^T\boldsymbol{J}\dot{\boldsymbol{s}},\\
&\dot{V}_1 = \boldsymbol{s}^T\{-\boldsymbol{w}^{\times}\boldsymbol{J}\boldsymbol{w} - \boldsymbol{J}\dot{\boldsymbol{w}}_r + \boldsymbol{u} + \boldsymbol{d} + 0.5\boldsymbol{J}[a_2\boldsymbol{I} + a_1\varrho\\
&\quad\times\mathrm{diag}(|q_{e0}\boldsymbol{q}_{ev}|^{\varrho-1})][-\boldsymbol{q}_{ev}\boldsymbol{q}_{ev}^T + q_{e0}(q_{e0}\boldsymbol{I} + \boldsymbol{q}_{ev}^{\times})]\boldsymbol{w}_e\}.
\end{aligned}$$

Substituting $\boldsymbol{u}$ from (15) in the above equation to obtain

$$\begin{aligned}
\dot{V}_1 &= \boldsymbol{s}^T\{-k\boldsymbol{s} - \hat{\boldsymbol{d}} - \gamma\,\mathrm{sign}(\boldsymbol{s}) + \boldsymbol{d}\},\\
&= -k\boldsymbol{s}^T\boldsymbol{s} - \gamma\|\boldsymbol{s}\| + \boldsymbol{s}^T(\boldsymbol{d} - \hat{\boldsymbol{d}}),\\
&\leq -k\boldsymbol{s}^T\boldsymbol{s} - \gamma\|\boldsymbol{s}\| + \|\boldsymbol{s}\|\|\tilde{\boldsymbol{d}}\|,\\
&= -k\|\boldsymbol{s}\|^2 - (\gamma - \|\tilde{\boldsymbol{d}}\|)\|\boldsymbol{s}\|.
\end{aligned} \tag{17}$$

By selecting the gain γ such that $(\gamma - \|\tilde{\boldsymbol{d}}\|) = \sigma > 0$, the equation (17) can be written as

$$\dot{V}_1 \leq -k\|\boldsymbol{s}\|^2 - \sigma\|\boldsymbol{s}\|. \tag{18}$$

Using the Property 1, $\|\boldsymbol{s}\|^2$ and $\|\boldsymbol{s}\|$ can be represented as

$$\|\boldsymbol{s}\|^2 \leq \frac{2}{\lambda_{\min}(\boldsymbol{J})}\left(\frac{\boldsymbol{s}^T\boldsymbol{J}\boldsymbol{s}}{2}\right);\ \|\boldsymbol{s}\| \leq \sqrt{\frac{2}{\lambda_{\min}(\boldsymbol{J})}}\left(\frac{\boldsymbol{s}^T\boldsymbol{J}\boldsymbol{s}}{2}\right)^{\frac{1}{2}}.$$

Applying (16) in the upper bound values of $\|\boldsymbol{s}\|^2$ and $\|\boldsymbol{s}\|$ and then substituting it in (18) to obtain

$$\dot{V}_1 \leq -\frac{2k}{\lambda_{\min}(\boldsymbol{J})}V_1 - \sigma\sqrt{\frac{2}{\lambda_{\min}(\boldsymbol{J})}}V_1^{\frac{1}{2}},$$

$$\dot{V}_1 \leq -\upsilon_1 V_1 - \upsilon_2 V_1^{\frac{1}{2}}, \tag{19}$$

where $\upsilon_1 = \frac{2k}{\lambda_{\min}(\boldsymbol{J})} > 0$, $\upsilon_2 = \sigma\sqrt{\frac{2}{\lambda_{\min}(\boldsymbol{J})}} > 0$. The equation (19) satisfies the relation given in *Lemma 1*. Therefore, the sliding surface will converge to zero in finite-time, i.e., the sliding mode will achieve in finite-time.

Proof (ii). Once $\boldsymbol{s} = 0$, then the following equation can be obtained from (13) as

$$\boldsymbol{w}_e = -a_1\mathbf{sgn}^{\varrho}(q_{e0}\boldsymbol{q}_{ev}) - a_2(q_{e0}\boldsymbol{q}_{ev}). \tag{20}$$

Lets consider another Lyapunov function $V_2 = \boldsymbol{q}_{ev}^T\boldsymbol{q}_{ev}$. The time derivative of V_2 yields

$$\dot{V}_2 = 2\boldsymbol{q}_{ev}^T\dot{\boldsymbol{q}}_{ev}. \tag{21}$$

Putting the value of $\dot{\boldsymbol{q}}_{ev}$ from (4b) in (21)

$$\dot{V}_2 = \boldsymbol{q}_{ev}^T\{(q_{e0}\boldsymbol{I} + \boldsymbol{q}_{ev}^{\times})\boldsymbol{w}_e\}. \tag{22}$$

Substituting the value of $\boldsymbol{w}_e$ from (20) in (22) to get

$$\dot{V}_2 = \boldsymbol{q}_{ev}^T(q_{e0}\boldsymbol{I} + \boldsymbol{q}_{ev}^{\times})\{-a_1\mathbf{sgn}^{\varrho}(q_{e0}\boldsymbol{q}_{ev}) - a_2(q_{e0}\boldsymbol{q}_{ev})\}. \tag{23}$$

Applying the skew-symmetric matrix property in (23), i.e., $\boldsymbol{q}_{ev}^T\boldsymbol{q}_{ev}^{\times} = 0$ (Tiwari et al., 2018), which gives

$$\begin{aligned}
\dot{V}_2 &= q_{e0}\boldsymbol{q}_{ev}^T\{-a_1\mathbf{sgn}^{\varrho}(q_{e0}\boldsymbol{q}_{ev}) - a_2(q_{e0}\boldsymbol{q}_{ev})\},\\
&= -a_1 q_{e0}\boldsymbol{q}_{ev}^T\mathbf{sgn}^{\varrho}(q_{e0}\boldsymbol{q}_{ev}) - a_2(q_{e0})^2\boldsymbol{q}_{ev}^T\boldsymbol{q}_{ev},\\
&= -a_1\sum_{i=1}^{3} q_{e0}q_{ei}|q_{e0}q_{ei}|^{\varrho}\mathrm{sign}(q_{e0}q_{ei}) - a_2(q_{e0})^2\boldsymbol{q}_{ev}^T\boldsymbol{q}_{ev},\\
&= -a_1\sum_{i=1}^{3}|q_{e0}q_{ei}|^{\varrho+1} - a_2(q_{e0})^2\boldsymbol{q}_{ev}^T\boldsymbol{q}_{ev},\\
&\leq -a_1|q_{e0}|^{\varrho+1}\sum_{i=1}^{3}|q_{ei}|^{\varrho+1} - a_2(q_{e0})^2V_2,\\
&\leq -a_1|q_{e0}|^{\varrho+1}V_2^{\frac{\varrho+1}{2}} - a_2(q_{e0})^2V_2,\\
&\leq -\eta_1 V_2^{\frac{\varrho+1}{2}} - \eta_2 V_2,
\end{aligned} \tag{24}$$

where $\eta_1 = a_1|q_{e0}|^{\varrho+1} > 0$, $\eta_2 = a_2(q_{e0})^2 > 0$. It is important to note that $q_{e0} = 0$ is not a stable equilibrium point (Jin and Sun, 2008). Again, according to *Lemma 1*, it shows that the relative vector quaternions are also converging to zero in finite-time. From the unity constraint, as $\boldsymbol{q}_{ev} \to 0$, $q_{e0} \to 1$. Since $\boldsymbol{q}_{ev}$ is converging to zero, therefore from the relation (20), $\boldsymbol{w}_e$ also goes to zero in finite-time. The proof is complete. □

Remark 1. The actuator input torque has the upper limit, i.e., $|u_i| \leq 10$ N.m where $i = 1, 2, 3$.

5. SIMULATION RESULTS

In this section, the proposed attitude tracking control is employed using numerical simulation to the rigid spacecraft model whose inertia matrix is

$$\boldsymbol{J} = [147\ 6.5\ 6; 6.5\ 158\ 5.5; 6\ 5.5\ 137]\ \text{kg.m}^2.$$

The external disturbances with random noises are considered as:

$$\boldsymbol{d}(t) = 10^{-2} \times \begin{bmatrix} +1 + 2\sin(0.5t) \\ -1 - 5\cos(0.5t) \\ +2 - 4\sin(0.5t) \end{bmatrix} + 5 \times 10^{-4}\begin{bmatrix} r \\ r \\ r \end{bmatrix} \quad \text{N.m.}$$

where r represents the white noise with variance 1.

Table 1. Initial conditions of states system & RNDO.

States	Value	States	Value
$\boldsymbol{q}_r(0)$	$[1\ 0\ 0\ 0]^T$	$\boldsymbol{q}(0)$	$[0.806\ 0.5587\ 0.105\ -0.1647]^T$
$\boldsymbol{w}_r(0)$	$[0\ 0\ 0]^T$	$\boldsymbol{w}(0)$	$[0\ 0\ 0]^T$
$\hat{\boldsymbol{d}}(0)$	$[0\ 0\ 0]^T$	$\boldsymbol{z}(0)$	$[0\ 0\ 0]^T$

Table 2. Parameters of the proposed control scheme.

Parameters	Value	Parameters	Value
μ_1	40	μ_2	2
ρ	0.9	ϱ	0.9
a_1	0.6	a_2	0.5
k	150	γ	0.005

All the initial conditions of system and RNDO dynamics are tabulated in Table 1. The parameters of the proposed control scheme are given in Table 2.

The performance of the RNDO is presented in Fig. 2 and 3. In Fig. 2, the actual disturbance $\boldsymbol{d}$ and the estimated disturbance $\hat{\boldsymbol{d}}$ from the RNDO are illustrated. As it can be seen from the zoomed-in plot of Fig. 2, the estimated disturbance $\hat{\boldsymbol{d}}$ converges to the actual disturbance within 0.15s. Furthermore, the above observation is also visible in Fig. 3, where the error between the actual and the estimated disturbance is plotted. The disturbance estimation error converges to the small bound of zero within 0.15s. After 0.15s, there are residual errors in $\tilde{\boldsymbol{d}}$, and this is because of the high frequency noises in the disturbance. The discontinuous control of NSTSMC attenuates the effects of high-frequency noises on the closed-loop system.

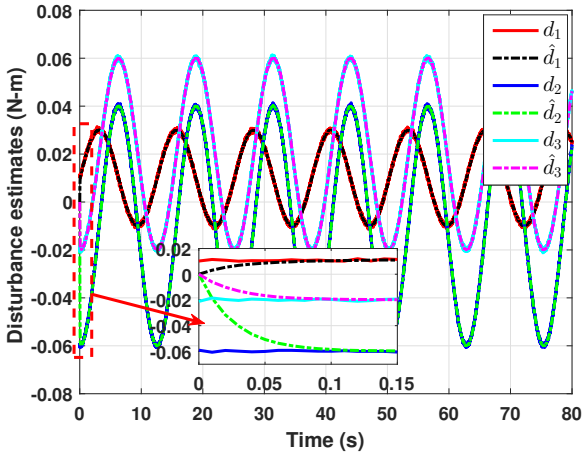

Fig. 2. Actual and estimated disturbances.

The plots of time-energy near-optimal reference angular velocity $\boldsymbol{w}_r$ and the body angular velocity $\boldsymbol{w}$ are shown in Fig. 4. The trajectory of $\boldsymbol{w}_r$ is generated using the LPSM technique, as discussed in Banerjee et al. (2019a). The reference trajectory $\boldsymbol{w}_r$ starts from rest and converges to zero in 37.13s. The body angular velocity tracks the reference trajectory within 14s while experiencing the disturbances and noises. The plot of relative angular velocity $\boldsymbol{w}_e$ is presented in Fig. 5. It is evident from the zoomed-in plot of Fig. 5 that $\boldsymbol{w}_e$ is converging to a small bound of 5×10^{-4} rad/s after 14s. Moreover, the steady-state convergence bound of $\boldsymbol{w}_e$ is 5×10^{-7} rad/s.

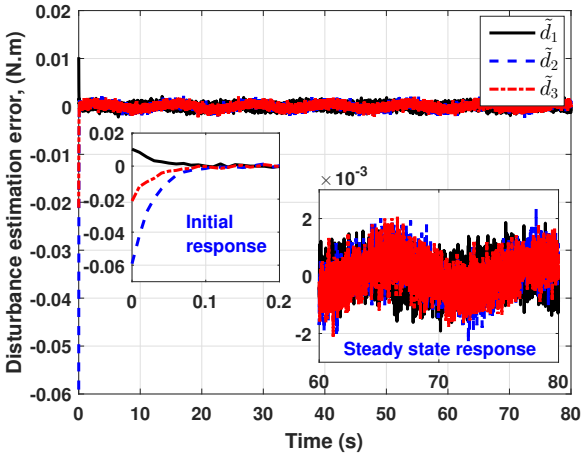

Fig. 3. Disturbance estimation error.

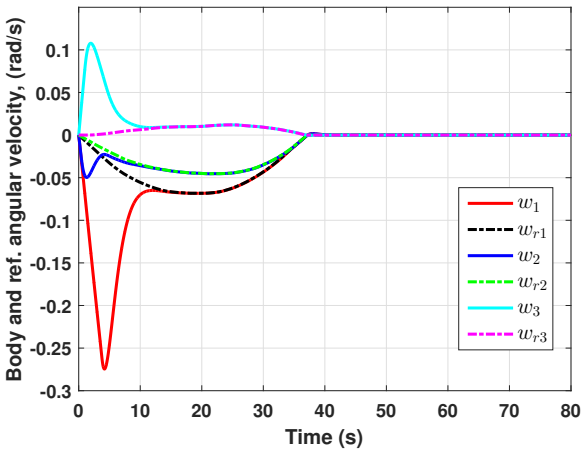

Fig. 4. Time-energy efficient reference angular velocity and body angular velocity.

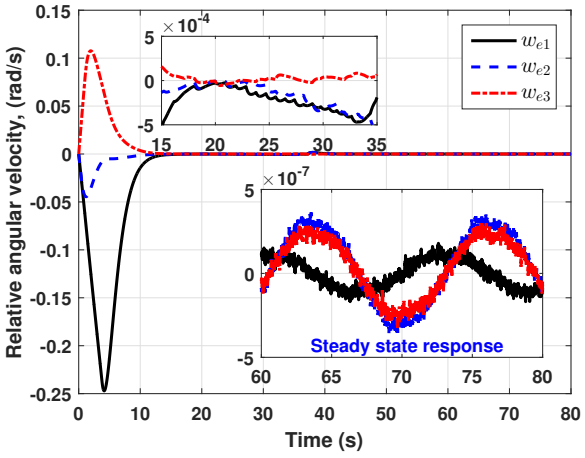

Fig. 5. Relative angular velocity response.

Trajectories of the relative quaternion are presented in Fig. 6. As it can be seen from Fig. 6 that the $\boldsymbol{q}_e$ is effectively converging to $[1\ 0\ 0\ 0]^T$ with the steady-state convergence bound of 5×10^{-7}. The sliding manifold of the NSTSS is demonstrated in Fig. 7. The settling time of

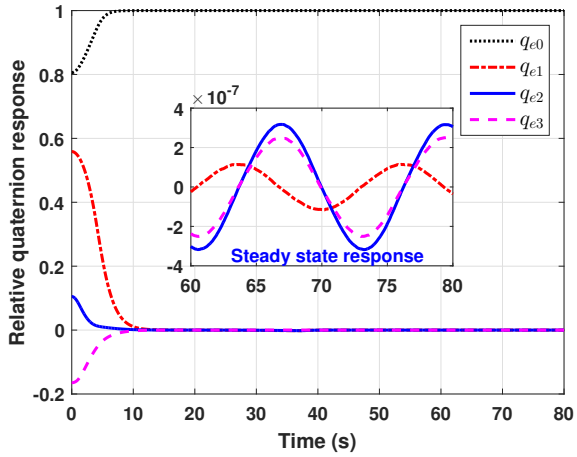

Fig. 6. Relative quaternion response.

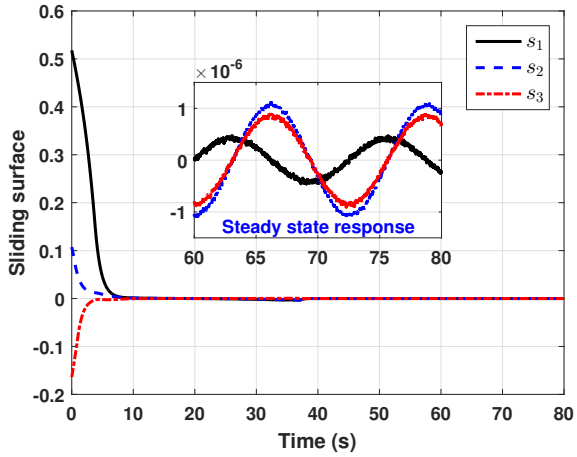

Fig. 7. Trajectories of sliding manifold.

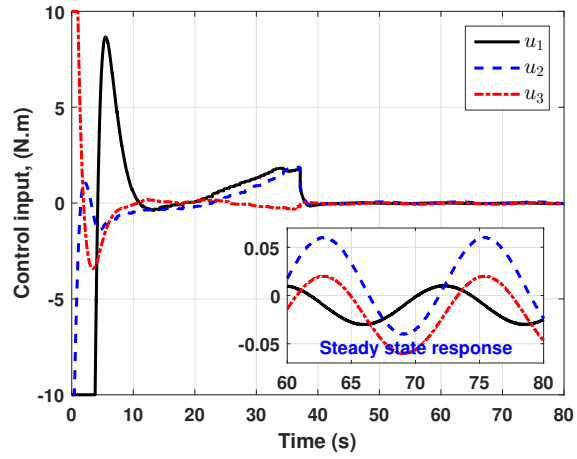

Fig. 8. Profile of control torque response.

$\boldsymbol{s}$ is within 8s, and the convergence bound of $\boldsymbol{s}$ during the steady-state is within 2.5×10^{-6}.

Plot of the proposed control torque is shown in Fig. 8. The torque has a saturation value of 10 N.m, and even under the saturated input, the proposed controller is effectively tracking the reference trajectory. The settling time of the

control response is 38s, and during the steady-state, the control input has a small magnitude of the order 10×10^{-2} N.m for rejecting the disturbances and noises in the system. Moreover, due to the use of RNDO, the proposed controller significantly alleviates the chattering from its control response by avoiding the use of high gain in the switching control.

Therefore, in light of the aforementioned performance results and discussions, the proposed controller (15) is effectively tracking the time-energy near-optimal reference attitude while rejecting the disturbances and alleviating the chattering.

6. CONCLUSION

This paper presents a robust composite control using an RNDO and NSTSMC for the spacecraft to track a time-energy near-optimal attitude generated by the LPSM. The spacecraft system, which is subjected to the disturbances, employs the RNDO for estimating the disturbance in finite-time and then feed it to the proposed controller for disturbance attenuation. The NSTSMC helps in ensuring the convergence of sliding manifold in finite-time and also forces the relative attitude states to their equilibrium points in finite-time. The numerical analysis of the closed-loop system validates the proposed strategy and illustrates the effective performance of the developed methodology.

REFERENCES

Amrr, S.M. and Nabi, M. (2019). Attitude stabilization of flexible spacecraft under limited communication with reinforced robustness. *Trans. of the Inst. of Meas. and Cont.*, 41(16), 4475–4487.

Amrr, S.M., Nabi, M., and Iqbal, A. (2019). An event-triggered robust attitude control of flexible spacecraft with modified rodrigues parameters under limited communication. *IEEE Access*, 7, 93198–93211.

Banerjee, A., Amrr, S.M., and Nabi, M. (2019a). Legendre-pseudospectral method based attitude control for tracking and regulation of rigid spacecraft. In *IEEE proc. 5th Ind. Cont. Conf. (ICC), New Delhi, India*, 347–352.

Banerjee, A., Amrr, S.M., and Nabi, M. (2019b). A pseudospectral method based robust-optimal attitude control strategy for spacecraft. *Adv. in Space Res.*, 64(9), 1688–1700.

Banerjee, A., Nabi, M., and Raghunathan, T. (2020). Time-energy optimal guidance strategy for realistic interceptor using pseudospectral method. *Trans. of the Inst. of Meas. and Cont.*, Early Access, 1–11.

Eshghi, S. and Varatharajoo, R. (2018). Nonsingular terminal sliding mode control technique for attitude tracking problem of a small satellite with combined energy and attitude control system (ceacs). *Aer. Sci. and Tech.*, 76, 14–26.

Feng, W., Han, L., Shi, L., Zhao, D., and Yang, K. (2016). Optimal control for a cooperative rendezvous between two spacecraft from determined orbits. *Jour. of the Astr. Sci.*, 63(1), 23–46.

Garg, D., Patterson, M., Hager, W.W., Rao, A.V., Benson, D.A., and Huntington, G.T. (2010). A unified framework for the numerical solution of optimal control problems using pseudospectral methods. *Automatica*, 46(11), 1843–1851.

Ge, X., Yi, Z., and Chen, L. (2017). Optimal control of attitude for coupled-rigid-body spacecraft via chebyshev-gauss pseudospectral method. *Appl. Math. and Mech.*, 38(9), 1257–1272.

Jin, E. and Sun, Z. (2008). Robust controllers design with finite time convergence for rigid spacecraft attitude tracking control. *Aer. Sci. and Tech.*, 12(4), 324–330.

Krstic, M. and Tsiotras, P. (1999). Inverse optimal stabilization of a rigid spacecraft. *IEEE Trans. on Aut. Cont.*, 44(5), 1042–1049.

Luo, W., Chu, Y.C., and Ling, K.V. (2005a). H-infinity inverse optimal attitude-tracking control of rigid spacecraft. *Jour. of Guid. Cont and Dyn.*, 28(3), 481–494.

Luo, W., Chu, Y.C., and Ling, K.V. (2005b). Inverse optimal adaptive control for attitude tracking of spacecraft. *IEEE Trans. on Aut. Cont.*, 50(11), 1639–1654.

Ma, K. (2013). Comments on "quasi-continuous higher order sliding-mode controllers for spacecraft-attitude-tracking maneuvers". *IEEE Tran. on Ind. Elect.*, 60(7), 2771–2773.

Qiao, J., Li, Z., Xu, J., and Yu, X. (2020). Composite nonsingular terminal sliding mode attitude controller for spacecraft with actuator dynamics under matched and mismatched disturbances. *IEEE Tran. on Ind. Inf.*, 16(2), 1153–1162.

Sahoo, A., Xu, H., and Jagannathan, S. (2016). Adaptive neural network-based event-triggered control of single-input single-output nonlinear discrete-time systems. *IEEE Trn. N. Net. Lear. Sys.*, 27(1), 151–164.

Strang, G. (1993). *Introduction to Linear Algebra*, volume 3. Wellesley-Cambridge Press Wellesley, MA.

Taheri, E. and Junkins, J.L. (2018). Generic smoothing for optimal bang-off-bang spacecraft maneuvers. *Jour. of Guid. Cont and Dyn.*, 41(11), 2470–2475.

Tiwari, P.M., Janardhanan, S., and un Nabi, M. (2018). Spacecraft anti-unwinding attitude control using second-order sliding mode. *Asian Jour. of Cont.*, 20(1), 455–468.

Wu, B. and Cao, X. (2017). Robust attitude tracking control for spacecraft with quantized torques. *IEEE Trans. on Aer. and Elect. Sys.*, 54(2), 1020–1028.

Yan, R. and Wu, Z. (2017). Spacecraft attitude tracking via robust disturbance observer. In *IEEE proc. 2017 29th Chin. Cont. And Dec. Conf. (CCDC), Chongqing, China*, 7415–7420.

Yu, S., Yu, X., Shirinzadeh, B., and Man, Z. (2005). Continuous finite-time control for robotic manipulators with terminal sliding mode. *Automatica*, 41(11), 1957–1964.

Zhou, H., Wang, D., Wu, B., and Poh, E.K. (2012). Time-optimal reorientation for rigid satellite with reaction wheels. *Inter. Jour. of Cont.*, 85(10), 1452–1463.

Zhu, Z., Xia, Y., and Fu, M. (2011). Adaptive sliding mode control for attitude stabilization with actuator saturation. *IEEE Tr. Ind. Elec.*, 58(10), 4898–4907.